SEVENTH EUROPEAN ROTORCRAFT AND POWERED LIFT AIRCRAFT FORUM

Paper No. 48

SEPARATED FLOW AROUND HELICOPTER BODIES

Polz, G.
Quentin, J.

Messerschmitt-Bölkow-Blohm GmbH
Munich, Germany

September 8 - 11, 1981

Garmisch-Partenkirchen
Federal Republic of Germany

Deutsche Gesellschaft für Luft- und Raumfahrt e.V.
Goethestr. 10, D-5000 Köln 51, F.R.G.

Paper No. 48 "Separated Flow Around Helicopter Bodies"

ERRATA

p. 5: line before eq. (1) "U outside"

p. 6: line next to the last: for "accurs" should read "occurs"

p. 7: eq. (6): for "γ" should read "r"

line before eq. (7) "velocity deficit ΔU"

p. 8: 6th line after eq. (8): "vorticity ω (fig. 8)"

p. 10: 3rd line: "streamline starting points"

section after fig. 10 should be replaced by

The origin of the trailed vorticity is assumed in the boundary layer of the fuselage similar to the shed vorticity (fig. 5). Owing to the inclination of the "wake body" against the free stream direction, the velocity vector U_s at the separation line outside the boundary layer has a circumferential component $U_s \cdot \sin \alpha_i$, which is equivalent to the vorticity in the boundary layer. This vorticity can be considered as the trailed vorticity, which occurs only in connection with a lift force. The trailed vortex system is deflected down (or up) against the free stream direction by the angle α_i. For the first iteration loop α_i is assumed as

p. 11.: line before eq. (11): for "on" should read "and"

p. 17: 11th line: for "make" should read "wake"

SEPARATED FLOW AROUND HELICOPTER BODIES

Polz, G.

Quentin, J.

Messerschmitt-Bölkow-Blohm GmbH

Munich, Germany

Abstract

On the rear part of the helicopter fuselage, flow separation is often unavoidable owing to the shape of the afterbody which is often defined more in accordance with operational requirements (for example cargo door) and with only minor consideration to aerodynamic aspects. Because of the separated flow, an analytical calculation of the flow-field using potential flow theory is not possible.

After an overview about the separated flow phenomena a method is explained based on a combination of panel methods with boundary layer analysis. In this method the wake flow region is represented by a wake body which consists of a uniformly distributed vorticity.

Calculated pressure distributions and flow fields are shown in comparison with wind tunnel test results. The main interest lies in the more downstream part of the wake, which is very important for the tail surface and tail rotor effectiveness.

Subject section: aerodynamics

1. Introduction

The design of helicopter fuselage bodies is influenced mainly by operational conditions; this leads to very different shapes (fig. 1), which are in generally not optimized from the aerodynamic point of view, so that flow separation on the rear part of the body is often unavoidable . The flow separation can result in high drag (and therefore penalize the maximum speed and fuel consumption) as well as poor stability and high vibration level. As the design trend in the helicopter

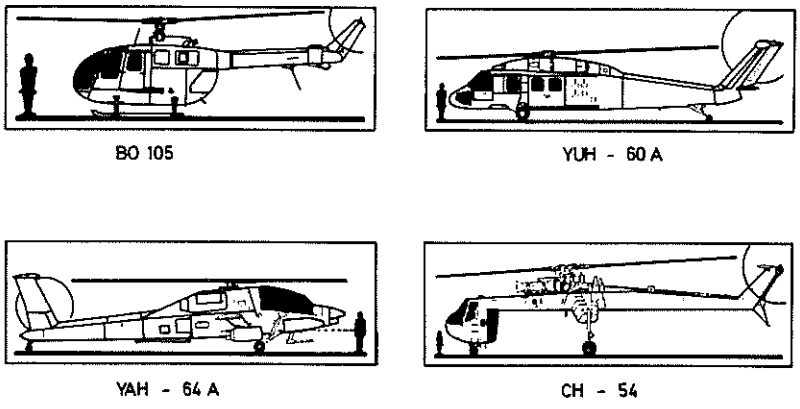

Fig. 1: Typical helicopter airframe configurations

development is for higher speeds, the problem of flow separation becomes more and more important. This has been the reason for a number of investigations in the recent years; partly experimentally, to investigate the behavior of actual configurations [1,2] ; partly theoretically, to give an insight into the phenomena of flow separation and to develop proper analytical methods [3 to 9] .

2. Aerodynamic effects and computation problems of separated flows

Flow separation in general, means that a region of highly distorted flow occurs at the rear side of fuselage. The main effects of the separation on the helicopter fuselage are (fig. 2)

- low static pressure on the rear side increases the drag
- sharp changes of local flow direction and
- reduced dynamic pressure in the wake influence the effectiveness of tailplane and tail rotor and therefore the stability of the aircraft.

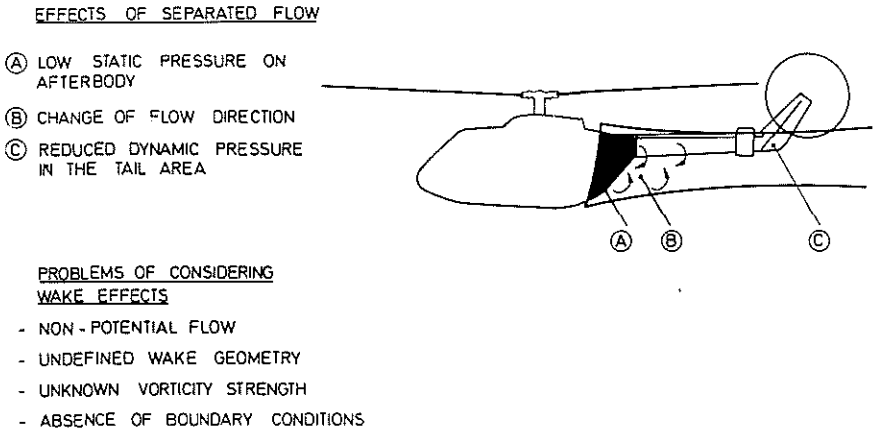

Fig. 2: Effects of flow separation and problems with their calculation

An analytical calculation of flow around the helicopter body, including the separated flow region with potential methods, is not possible because of the viscous character of the separated flow. A simulation of this type of flow is however possible by the use of vortex elements, but it is impaired by the following difficulties

- the unknown wake geometry

- the unknown vorticity strength

- the absence of any boundary conditions

This is in contrast to fixed wing aerodynamics where the unknown vorticity strength can be calculated by the use of known wake geometry with the help of the Kutta-Joukowsky boundary conditions.

3. Analysis of the separated flow on fuselage bodies

Two examples of flow separation on the aft body of a helicopter fuselage are shown in fig. 3. While the BK117-model shows a rather small area of flow separation, but indicates clearly the presence of the vortex pair associated with the fuselage lift, the experimental helicopter model (which has been designed especially for flow separation studies) has a rather large separated area.

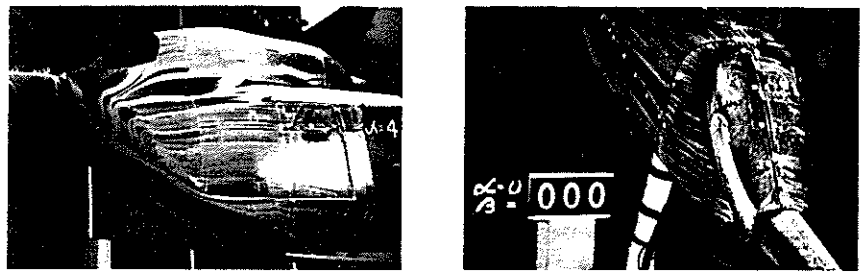

BK 117 ($\alpha = 4°$, $\beta = 0°$)

EXPERIMENTAL HELICOPTER MODEL

Fig. 3: Typical flow separation on helicopter fuselage

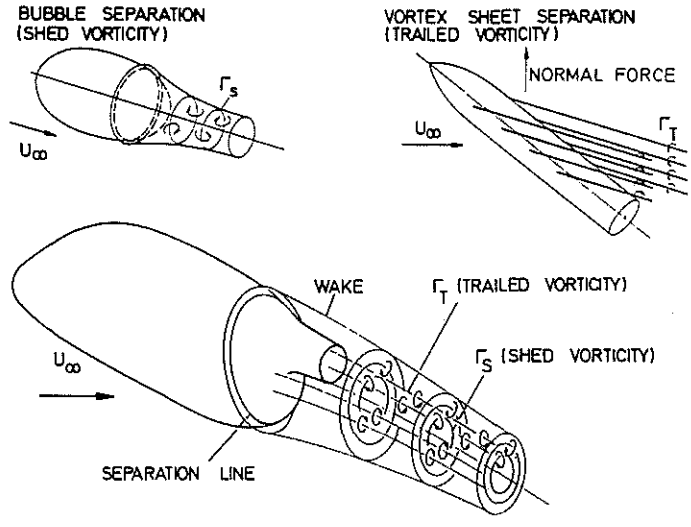

Fig. 4: Types of separated flow

From the oil flow pictures it can be seen, that real separated flows consist of a combination of (fig. 4)

- pure bubble separation with vorticity "shedding" from the circumferential separation line; since it typically occurs on axial-symmetric blunt bodies

- slender body separation with vorticity "trailing" from a more longitudinal separation line combined with a normal force.

Both types of separation create a region of reduced pressure at the rear side of the body.

3.1 Origin of the wake vorticity

It is known that the origin of the wake vorticity lies in the boundary layer on the body surface (fig. 5).

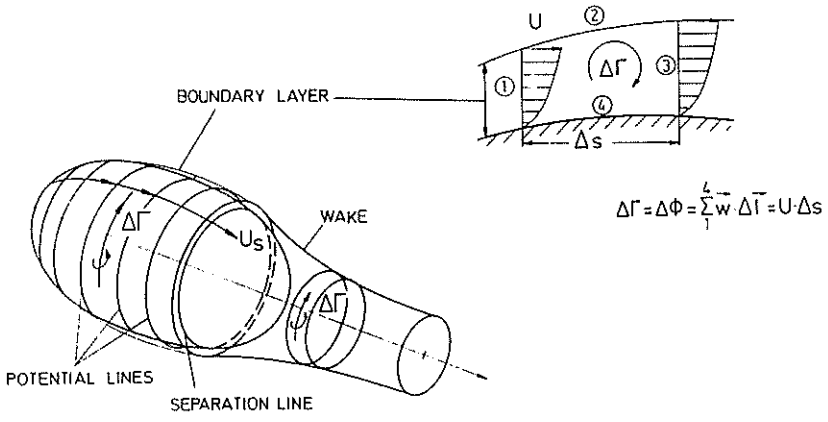

Fig. 5: Origin of wake vorticity

The vorticity linked with a streamline element Δs is equal to the velocity potential $\Delta\phi$, which is a function of the local velocity outside the boundary layer.

$$\Delta\Gamma = \Delta\phi = \oint \vec{w} \cdot d\vec{s} = U \cdot \Delta s \qquad (1)$$

is independent from the velocity profile, but the vorticity distribution across the boundary layer thickness $\omega(z)$ is proportional to the velocity gradient $\partial u/\partial z$ (chap. 3.2). The vorticity distribution over the streamline length is

$$\gamma = \frac{\partial\Gamma}{\partial s} = 2 \int_0^{\delta} \omega(z) \cdot dz = \int_0^{\delta} \frac{\partial u}{\partial z}\, dz = U \qquad (2)$$

Thus the vorticity transport across the separation line into the wake is

$$\frac{\partial\Gamma_s}{\partial t} = \int_0^{\delta_s} \frac{\partial u}{\partial z}\, u\, dz = \frac{U^2_s}{2} \qquad (3)$$

This is the only origin for the shed vorticity in the wake.

A similar behavior is noticeable for the trailed vorticity, which occurs in the case of non-rotational symmetric flow. Oil flow studies show that, for bodies that are not extremely slender, no additional separation line exists for the trailed vorticity, which is found only to occure downstream from the separation line of the shed vorticity.

3.2 Vorticity distribution in the wake

The vorticity distribution in the wake is generally unknown. The only possible solution is based on the use of the velocity distribution via the Euler equations. From the complete equation for rotating flow

$$\vec{\omega} = \begin{vmatrix} \omega_x \\ \omega_y \\ \omega_z \end{vmatrix} = \frac{1}{2} \begin{vmatrix} \frac{\partial w}{\partial y} - \frac{\partial v}{\partial z} \\ \frac{\partial u}{\partial z} - \frac{\partial w}{\partial x} \\ \frac{\partial v}{\partial x} - \frac{\partial u}{\partial y} \end{vmatrix} \tag{4}$$

only the second component is important for the shed vorticity in a plane through the wake centerline. As the normal velocity component w is subjected

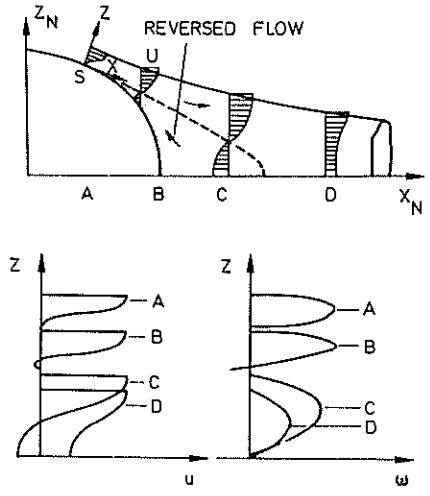

Fig. 6: Distribution of wake velocity and vorticity

to small changes over the x-direction, the rotation at the shed vorticity is

$$\omega_y = \frac{1}{2} \left(\frac{\partial u}{\partial z} - \cancel{\frac{\partial w}{\partial x}} \right) = \frac{1}{2} \frac{\partial u}{\partial z} \tag{5}$$

In fig. 6, for several stations in the wake, the velocity and the resultant vorticity distributions are qualitatively shown over the wake radius. At the separation line (station A), the velocity profile is almost sinusoidal and the respective vorticity profile approximately parabolic. A similar shape accurs at station B except for the inner part of the profile, where the boundary layer to the reverse flow

creates an opposite rotating vorticity. The reverse flow alone (station B and C) does not influence the shape of the vorticity distribution, but only the vorticity strength. At station D the vorticity decay caused by the viscosity is visible.

3.3 Wake geometry

One of the main points of interest in the investigation of separated flows is the shape of the wake. Its outer surface is defined as the boundary between the viscous flow and the potential flow with constant total energy. Just as in the case at the boundary layer, along each streamline additional mass from the outer flow is continually entrained in the wake. Thus the wake diameter grows more and more compared with the streamlines, which form the outer wake boundary at the separation line (fig. 7).

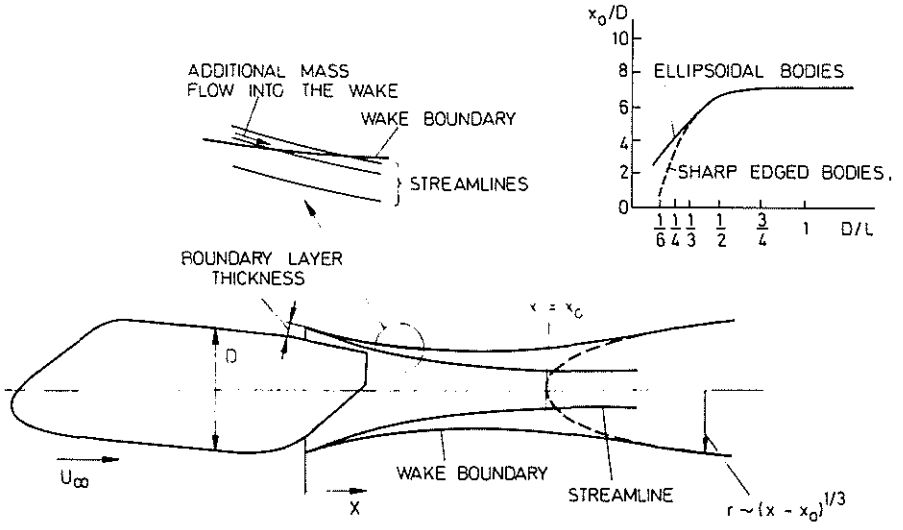

Fig. 7: Wake geometry

At greater distances from the separation line, where the displacement effect of the body has nearly vanished the shape of an axisymmetric wake can be expressed by the equation

$$\gamma \sim (x-x_o)^{1/3} \tag{6}$$

which comes from Prandtl's mixing layer theory for turbulent flows. The basis of this theory is a constant momentum difference between the wake and the outer flow which is equal to the drag of the body. Since for the wholewake the same shape of the velocity profile can be assumed (fig. 6), the momentum difference is the product of the cross sectional area and the maximum velocity deficit in the wake. This leads to the relation

$$\Delta U \sim \frac{\text{momentum loss}}{\text{cross sectional area}} \sim (x-x_o)^{-2/3} \tag{7}$$

between ΔU and r , which is valid only for distances greater than x_o from the separation line. Experimental results (fig. 7) show that for rather blunt shapes of helicopter bodies x_o normally lies behind the tail end. For the region between the separation line and $x = x_o$ no proper experimental

results are available, but a smooth change-over of the outer wake boundary as shown in fig. 7 can be assumed here. The simple equation for the velocity deficit (eq. 7) is not valid any more in this region, because of the change of the static pressure. For the lifting case a similar behavior of the trailing vorticity can be assumed, since this vorticity remains within the wake boundary.

4. Computational method

Especially for helicopter aerodynamics, a method has been developed, with the main purpose of simulating the flow conditions further downstream from the separation line in the tail region.

4.1 Theoretical basis

The singularity methods, widely used in fluid mechanics, are based on a integral equation type as

$$\frac{\vec{n}}{4 \cdot \pi \cdot U_\infty} \nabla \iint_{(s)} \sigma(s) \frac{ds}{r(s,p)} = \vec{n} \cdot \frac{\vec{U}_\infty}{U_\infty} \qquad (8)$$

This integral equation can only be solved, when the body surface is divided into a number of panels, each with constant singularity strength. The solution is carried out usually by a linear equation system, which needs the same number of boundary conditions as number of panels considered.

In the case of separated flow the equation system should be extended by the influence of the wake vorticity (fig. 8). Since neither the geometry nor any of the boundary conditions are known for the wake vorticity, an iterative solution procedure is necessary, whereby the vorticity resulting

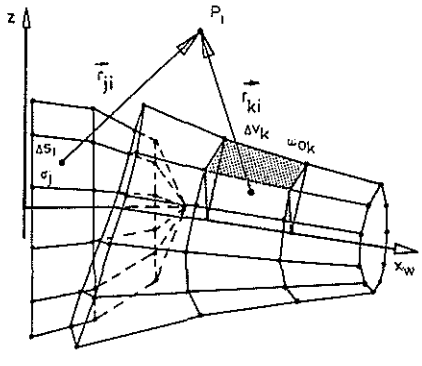

INTEGRAL EQUATION

$$\frac{\vec{n}}{4\pi U_\infty} \cdot \left[\nabla \iint_{(s)} \frac{\sigma(s)}{r(s,p)} ds + \iiint_{(v)} (\nabla) \frac{\vec{e}_r \times \vec{r}(v,p)}{r(v,p)^3} dv\right] = \vec{n} \cdot \frac{\vec{U}_\infty}{U_\infty}$$

SUMMATION EQUATION

$$\frac{\vec{n}}{4\pi U_\infty} \nabla \sum_{(s)} \frac{\sigma}{r} \Delta S = \vec{n} \left[\frac{\vec{U}_\infty}{U_\infty} - \frac{1}{4\pi U_\infty} \sum_{(v)} \frac{-\rho}{r^3} \cdot \Delta V\right]$$

NONLINEAR SYSTEM

$$[A_{ij}] \{x_j\} = \{B_i\}$$

$$A_{ij} = \vec{n}_i \; C_{ij}$$

$$x_j = \frac{\sigma_j}{4\pi U_\infty}$$

$$B_i = -\vec{n}_i \cdot \frac{\vec{U}_\infty}{U_\infty} + \vec{n} \sum_k \omega_{ok} \cdot \vec{D}_{ik}$$

Fig. 8: Numerical solution of the integral equation for separated flow

from the foregoing iteration loop is joined at the right side of the equation system. For the first iteration loop an adequate wake geometry and vorticity distribution has to be chosen.

4.2 Computer program system

The program system consists of a set of five separate computer programs (fig. 9) which is used in an iterative procedure. A well-known panel method [10,11] based on a source/sink-distribution of the body surface is used for the calculation of the displacement effects. From the given coordinates of the body surface the panel arrangement is generated. In the second step the source distribution is defined by the solution of the potential equation. The right side of the equation system consists of the tangential flow condition on each panel and the induced velocities of the wake from the foregoing iteration loop. By interpolation of the flow field on the body surface a number of body

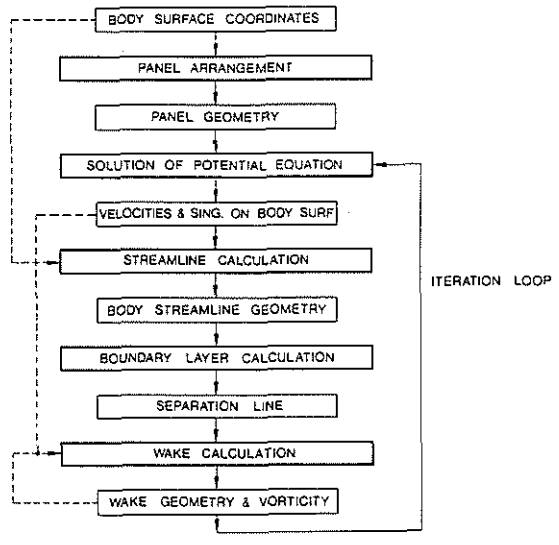

Fig. 9: Program outline for separated flow calculation method

streamlines is generated, each providing a separation point by a boundary layer calculation with a two-dimensional integral method [12] . The use of these method relies on the substitution of the real body by a rotational symmetric "replacement body" for each streamline. The "wake body" is attached at the separation line and its geometry and velocity distribution is influenced by the source distribution on the fuselage. The wake vorticity influences the source distribution in the next iteration loop. Reasonable results are achieved after two iteration loops.

For the first loop a wake body with constant cross section and constant wake vorticity, based on the boundary layer data at the separation line, is assumed.

4.3 Wake geometry and vorticity distribution

For the numerical calculation the wake geometry as well as the distribution for the trailed vorticity have to be defined. As is shown in section 3.3, the wake boundary can be determined by a number of lines beginning at the separation line with continually increasing distance to the accompanying streamline, and finally tangential joining to the boundary defined by equation (6). A good approximation is achieved by

$$r_w = r_s \, (1+m)^x \tag{9}$$

with m in the range from 0.02 ... 0.05 (fig. 10). For the first iteration loop the "wake body" cross section is assumed as constant, beginning from the stream line stating points at the separation line.

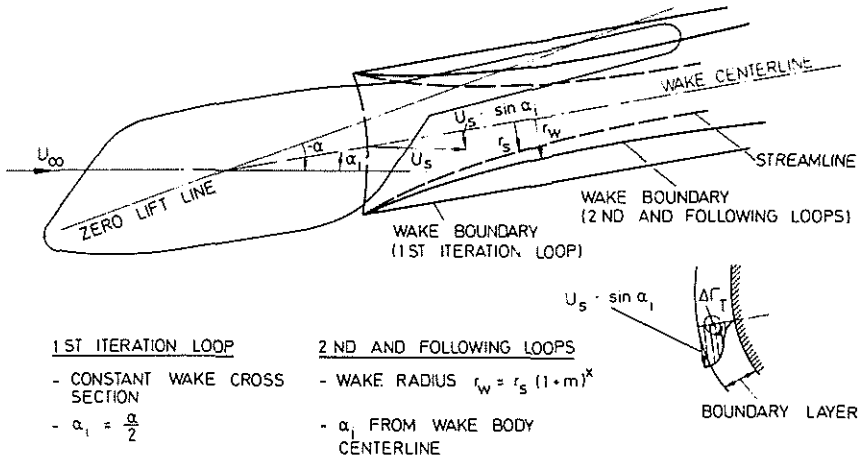

Fig. 10: Determination of wake geometry and trailed vorticity strength

The origin of the trailed vorticity is assumed in the boundary layer of the fuselage similar to be shed vorticity (fig. 5). Owing to the inclination of the "wake body" against the free stream direction, the velocity rector U_s at the separation line outside the boundary layer has a circumferential components $U_s \sin \alpha_i$ which is equivalent to the vorticity in the boundary layer. This vorticity can be considered as the trailed vorticity, which occurs only in connection with a lift force. The trailed vortex system is deflected down (or up) the wake axis by induced angle α_i . For the first iteration α_i is assumed as

$$\alpha_i = \frac{\alpha}{2} \tag{10}$$

the theoretical value for wings with aspect ratio approaching zero. Here α is the angle between the zero lift axis and the direction of the freestream velocity.

4.4 Wake discretization and calculation of vortex induced velocities

The geometry of the wake body is given by a number of surface lines arranged nearly equidistant around the circumference. Cross sections have a polygonial shape, which can be divided into triangular elements with the use of the wake body centerline. In the region of the fuselage the elements are of trapezoidal shape. All triangular elements of a cross section are covered with the same shed vorticity.

γ_s which is distributed over the actual radius of the element by a parabolic function (fig. 6). The geometric data and vorticity distribution of these elements are used for the calculation of the vortex induced velocities.

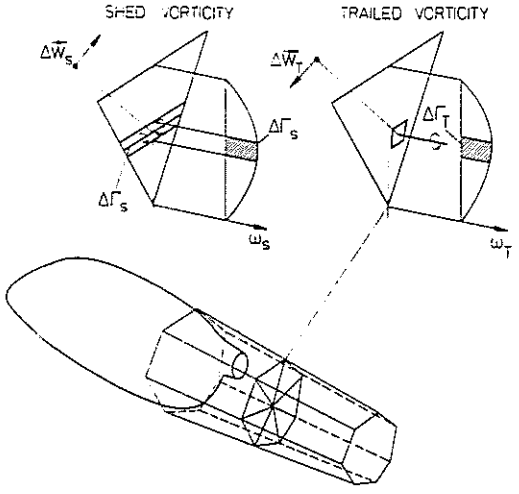

Fig. 11: Calculation of wake induced velocities

For the numerical procedure (fig. 11) the smoothly distributed vorticity is represented by a row of single line vortices, the number of which is dependent on the distance to the point, where the velocity has to be calculated.

The trailed vorticity orginating at the separation line is held constant along the wake body for each row of triangular elements. For the numerical calculation each triangular element is divided into a number of subelements, each represented by a line vortex. For the real vortex induced velocities the effects of all elements of a cross section are added together and then integrated over the wake body length with respect to the x-coordinate.

The wake body should be extended to a position about two diameters downstream from the last point, where the flow has to be calculated.

Inside the wake, the total pressure is reduced by the strength of the shed vorticity between the outer wake boundary on the considered position

$$Cp_{tot} = 1 - \gamma_s^2 \tag{11}$$

similary the static pressure depends on the vorticity strength

$$C_{ps} = 1 - \frac{U^2}{2} - \gamma_s^2 \tag{12}$$

5. Application of the method

The applicability of the calculation method is shown in several examples. As the main result, the pressure distributions on the rear part of the body and the flowfield in the region of the wake are obtained.

5.1 Flow field and pressure distribution on a sphere

In fig. 12 and 13 the flow field past a sphere and the inherent pressure distribution, calculated for a Reynolds number of $0.45 \cdot 10^6$ are presented. The pressure distribution is compared with measurements and the result for the unseparated potential flow, whereby the measurement is simulated satisfactorly by the separated flow model. Only a rather high pressure rise is noticeable near the separation line; it is caused by the front edge of the wake, which acts almost like a step for the oncoming flow. The flow field shows clearly the cavity flow region, and embedded in it the region of reversed flow.

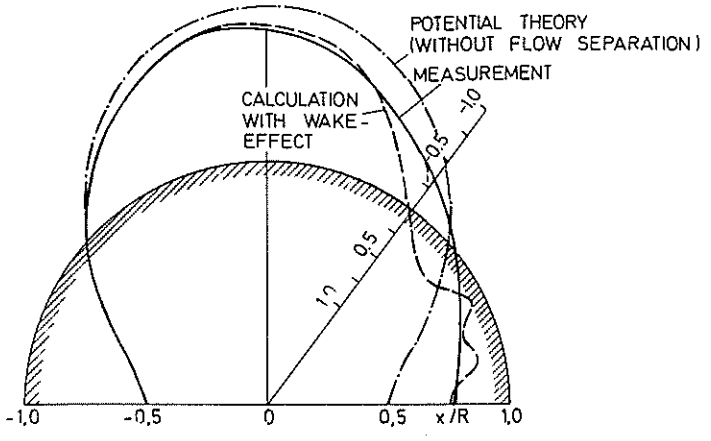

Fig. 12: Pressure distribution on a sphere, Reynolds number = $0.45 \cdot 10^6$ (calculation and measurement)

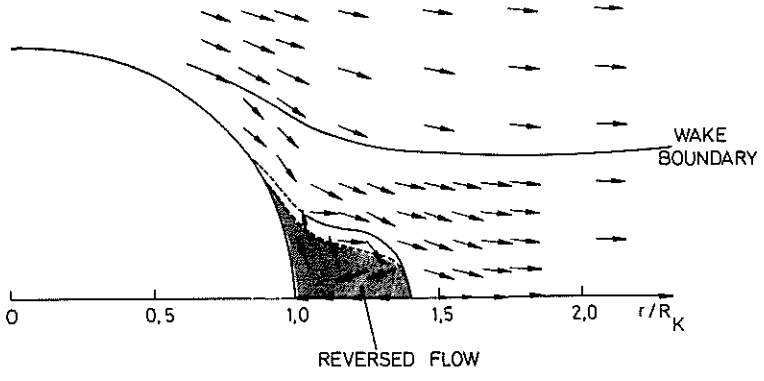

Fig.13: Velocity field of the separated flow past a sphere, Reynolds number = $0.45 \cdot 10^6$

5.2 Separated flow studies on an experimental helicopter model

For an experimental and theoretical study by MBB and the DFVLR about the influence of the fuselage shape on flow separation and wake structure [8] , an experimental helicopter fuselage model has been tested in a wind tunnel. In the first stage of the investigations a rather steep ramp angle on the after body had been chosen because of the possibility for cargo door loading (fig. 15). The studies have not yet been completed, but some initial experimental results, which were

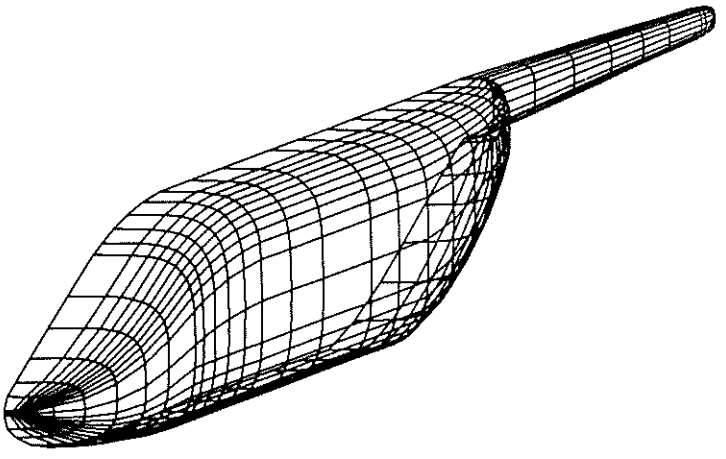

Fig. 14: Panel arrangement on the experimental helicopter model (half body)

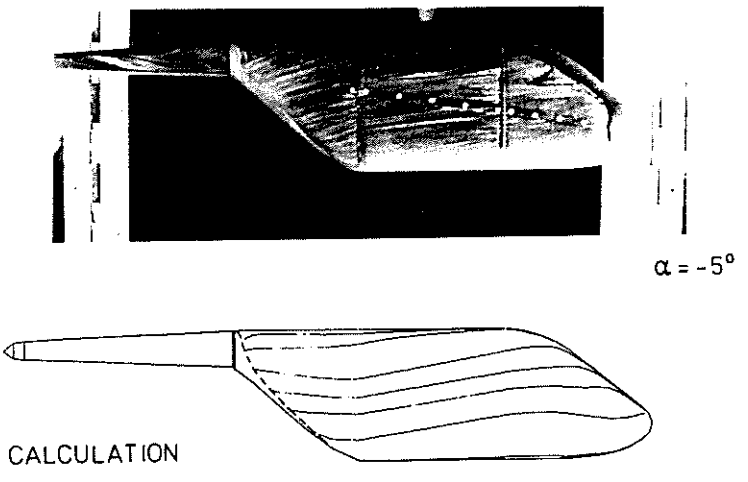

Fig. 15: Fuselage streamlines on experimental helicopter model (calculation and experiment)

achieved for an angle of attack of α = -5 deg (this is approximately the angle for cruising flight), have been simulated with the calculation model for separated flows. Fig. 14 shows the body shape and the arrangement of the total 1252 panels.

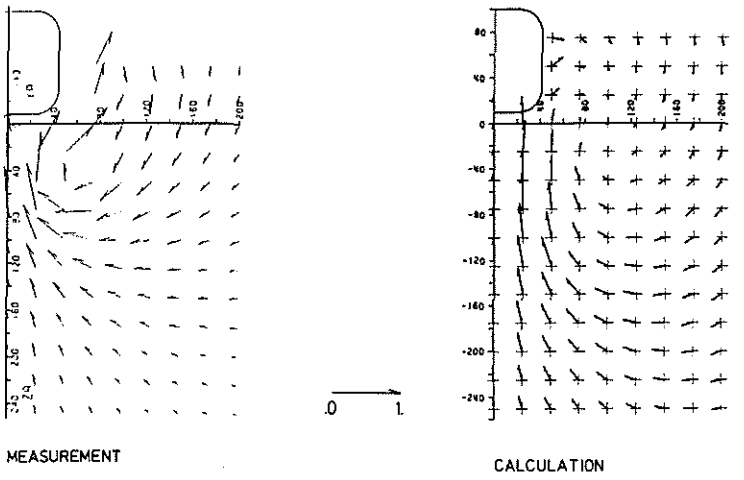

Fig. 16: Velocity field in the cross section at body-tailboom junction of the experimental helicopter model

In fig. 15 the calculated streamlines on the fuselage and the separation line are shown in conjunction with the experimental results for comparison. Whilst the separation lines are very similar, the calculated streamlines on the body are bent up rather sharply in the vicinity of the separation line, which can be credited to the use of the two-dimensional boundary layer model. However it should be noted, that the oil flow studies can only show the streamlines immediately adjacent the body surface "below" the boundary layer, while the calculation yields the potential flow streamlines outside the boundary layer.

In fig. 16 the velocity vector distribution in a wake cross section at the body-tailboom intersection is shown. The position and sense of rotation can be reproduced reasonably realistically by the calculation, but the model is not able to simulate the vortex roll up, even if the reduced velocity in the vortex core is visible. Fig. 17 shows the pressure

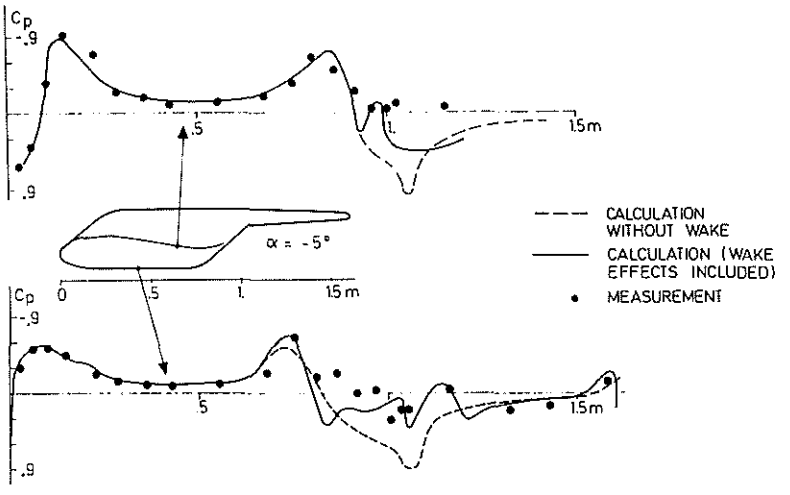

Fig. 17: Pressure distribution on experimental helicopter model

distribution along two streamlines on the fuselage. The agreement between the results, calculated with the separated flow model, and the measurement is in general quite good, especially in comparison with the pure potential model. A remarkable feature is an overlarge pressure increase in front of the separation line, where the front edge of the wake body influences the oncoming flow such as a step in the contour.

5.3 Wake structure and pressure distribution on BK117 wind tunnel test model

For a wind tunnel test model of the BK117 several experimental results are also simulated. In this case the fuselage was represented by about 1000 panels (fig. 18).

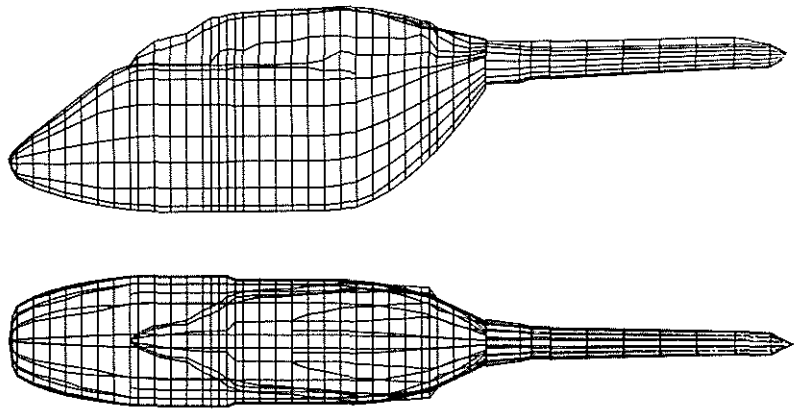

Fig. 18: Panel arrangement on BK117 wind tunnel model

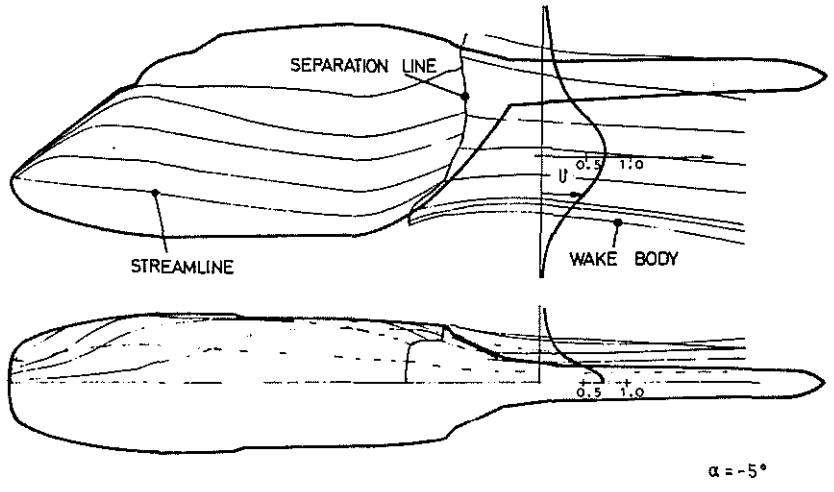

Fig. 19: Calculated flow around BK117 wind tunnel model

In fig. 19 the streamlines on the fuselage, the separation line and the wake body are presented for an angle of attack of -5 deg. At the rear

bottom of the fuselage the separation line was fixed by a small spoiler in this wind tunnel test. The spoiler was not taken into account in the calculation, but the separation line on this part of the fuselage was taken from the measurements. As fig. 19 shows, the momentum loss in the centre of the wake reaches about 70 % of the freestream velocity.

Although the velocity distribution across the wake is not comparable with experimental results, the drag evaluation from the momentum loss agrees very well with the measured value. Also the calculated pressure distribution, which is shown in fig. 20 for two lines along the fuselage, shows reasonable agreement with the experimental results.

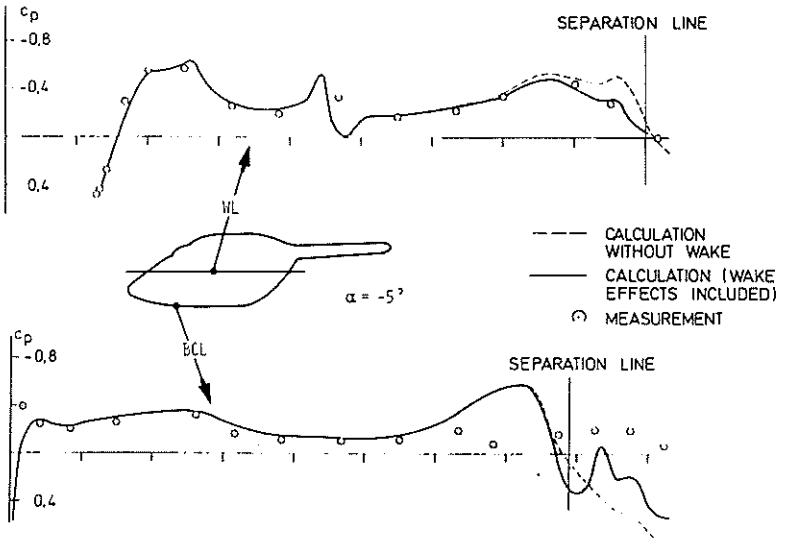

Fig. 20: Pressure distribution on BK117 wind tunnel model

The reason for the use of a spoiler is to prevent any movements of the separation line with changing of angle of attack, (which would greatly influence the aerodynamic forces on the fuselage), since then the BK117 spoiler has been replaced by a pair of fins providing a reduced drag with the same stability effects.

6. Conclusions

The problems of calculation of the separated flow on helicopter bodies have been demonstrated. After an overview of the main aerodynamic effects and the general calculation problems the separated flow is analysed with regard to the, in general, unknown wake characteristics, as e.g. geometry and vorticity, which is distributed in shed and trailed vortices.

A calculation model has been developed on the basis of an approved panel method and a boundary layer method. Explanation of the model concentrates on the determination of the wake geometry and vorticity. An iterative procedure is necessary to solve the main potential equation using the wake parameters from the foregoing iteration loop.

The applicability of the method is demonstrated on different body shapes. Pressure distributions and wake characteristics can be simulated to sufficient accuracy, although some improvements are desired. The calculation of separated flow suffers mainly from the lack of sufficient experimental results. In this area additional information is expected from the present wind tunnel activities.

For the calculation method several modifications seem to be convenient, such as replacement of the two-dimensional boundary layer model by a three-dimensional method. modelling of the trailed-vortex roll up, and smoothing of the step-like effect of the front edge of the wake body.

Another field for future studies is the modelling of the make of the main rotor hub area ar well as of the attachments that can prevent the adverse effects of flow separation, such as spoilers, strakes etc. However for further investigations in this area more experimental results are necessary.

7. References

1. P.F. Sheridan, R.P. Smith — Interactional Aerodynamics - A New Challenge to Helicopter Technology. 35th Annual National Forum of the American Helicopter Society, Preprint No 79-59

2. P. Roesch — Aerodynamic Design of the Aerospatiale SA365 N-Dauphine 2 Helicopter. 6th European Rotorcraft and Powered Lift Forum, Bristol 1980, Paper No. 28

3. F.A. Woodward, F.A. Dvorak, E.N. Geller — A Computer Program for Three-Dimensional Lifting Bodies in Subsion Inviscid Flow. USAAMRDL-TR-74-18

4. F.A. Dvorak, B. Maskew, F.A. Woodward — Investigation of Three-Dimensional Flow Separation of Fuselage Configurations. Final Report for Period May 1975 - May 1976 USAAMRDL-TR-77-4

5. D.R. Clark, F.A. Dvorak, B. Maskew, F.A. Woodward — Helicopter Flow Field Analysis. Final Report for Period April 1977-September 1978. USARTL-RT-79-4

6. D.R. Clark, F. Wilson — A Study of the Effect of Aft Fuselage Shape on Helicopter Drag. 6th European Rotorcraft and Powered Lift Aircraft Forum, Bristol 1980, Paper No. 50

7. R. Stricker, G. Polz — Calculation of the Viscous Flow Around Helicopter Bodies. 3rd European Rotorcraft and Powered Lift Aircraft Forum, Aix-en-Provence 1977, Paper No. 43

8. G. Polz, J. Quentin, A. Kühn — Windkanaluntersuchungen zur optimalen Gestaltung von Transporthubschauberzellen hinsichtlich Leistungsbedarf und Stabilitätsverhalten. MBB-Report UD-290-80, 1981

9. G. Polz — Zur Berechnung der abgelösten Strömung an Hubschrauberrümpfen. DGLR-Jahrestagung, Aachen 1981, Paper No.26

10. W. Kraus, P. Sacher — Das MBB-Unterschall-Panelverfahren. MBB-Reports UFE 637-70, UFE-633-70 and UFE-634-70, 1970

11. W. Kraus — Weiterentwicklung des Panelverfahrens. MBB-Report UFE 1017 (ö), 1973

12. J.C. Rotta — FORTRAN IV-Rechenprogramm für Grenzschichten bei kompressiblen, ebenen und achsensymmetrischen Strömungen. DFVLR-Report 71-51, 1971